A Notations

Notations	Descriptions
$\mathbf{DG} = \{\mathcal{G}\}_{t=1}^{T}$	Dynamic graph (a set of T discrete graph snapshots)
$\mathcal{G} = (\mathcal{V}, \mathcal{E})$	Graph with the node set $\mathcal{V}$ and edge set $\mathcal{E}$
$\mathcal{G}^t = (\mathcal{V}^t, \mathcal{E}^t)$	Graph snapshot at time t
$\mathbf{X}^t$, $\mathbf{A}^t$	Node features matrix and adjacency matrix of a graph at time t
$\mathbf{x}_v^t$, $\mathbf{A}_{(u,v),k}^t$	Node features and edge weights of (u, v) under $\mathbf{e}_k$
$\mathcal{G}^{1:t}$, Y^t, $\mathbf{G}^{1:t}$, $\mathbf{Y}^t$	Graph trajectory, labels and their corresponding random variables
$\mathbf{e}$, $\mathbf{e}_i$, $\mathbf{E}$	Latent environments and their support
$\mathbf{z}_{v,k}^t$, $\mathbf{z}_v^{\mathbf{e},t}$, $\mathbf{z}_v^{\mathbf{e}}$	Node representations under $\mathbf{e}_k$, at time t and at overall time slices
$\mathbf{z}$, $\mathbf{y}$	Observed environment sample with its label
d, d'	Dimension for $\mathbf{x}_v^t$ and $\mathbf{z}_{v,k}^t$, respectively
K	Number of underlying environments (number of convolution channel)
$f(\cdot)$, $w(\cdot)$, $g(\cdot)$	Model, encoder, and the link predictor
$\ell(\cdot)$	The loss function
q_ϕ, p_ω	The prior distribution and variational distribution of environments
$\mathbb{I}^\star(\cdot)$, $\mathbb{I}(\cdot)$	Invariant pattern recognition function and its implementation
$\mathcal{P}_{\mathbf{e}}^I$, $\mathcal{P}_{\mathbf{e}}^V$, $\mathcal{P}_{\mathbf{e}}^I(v)$, $\mathcal{P}_{\mathbf{e}}^V(v)$	Summary of spatio-temporal invariant/variant patterns for each node
$\mathbf{Z}^{1:t}$, $\mathbf{Z}_I^{1:t}$, $\mathbf{Z}_V^{1:t}$	Summary of node representations, and their variants under $\mathcal{P}_{\mathbf{e}}^I$ and $\mathcal{P}_{\mathbf{e}}^V$
$\mathcal{S}_{\text{ob}}$, $\mathcal{S}_{\text{ge}}$	Observed and generated environments sample libraries
s, $\mathbf{s}_v$	Intervention samples from $\mathcal{S}_{\text{ob}} \cup \mathcal{S}_{\text{ge}}$ and their summary for node v
$\text{do}(\cdot)$	*do*-caculus for causal interventions
$\mathcal{L}_{\text{task}}$, $\mathcal{L}_{\text{risk}}$, $\mathcal{L}_{\text{ECVAE}}$	Task loss, the invariance loss and the ECVAE loss
α, β	Hyperparameters for loss trade-off

B Algorithm and Complexity Analysis

Algorithm 1: Overall training process of EAGLE.

Input: Dynamic graph $\mathbf{DG} = (\{\mathcal{G}\}_{t=1}^{T})$ with labels $\mathbf{Y}^{1:T}$ of link occurrence; Number of training epochs E; Number of intervention times S; Hyperparameters α and β.

Output: Optimized model $f_{\boldsymbol{\theta}}^\star$; Predicted label Y^T of link occurrence at time $T+1$.

Initialize parameters randomly;
for $i = 1, 2, \cdots, E$ **do**
  `// Environments Modeling and Inferring`
  Obtain representations for each node at each time with the support of $\mathbf{e}$, as $\mathbf{z}_v^{\mathbf{e},t} \leftarrow$ Eq. (6);
  Establish the observed environment samples library $\mathcal{S}_{\text{ob}} \leftarrow$ Eq. (7);
  Infer the distribution $p_\omega(\mathbf{e})$ with $\mathcal{L}_{\text{ECVAE}} \leftarrow$ Eq. (8) and generate samples library $\mathcal{S}_{\text{ge}}$;
  `// Environments Extrapolating`
  Learn the invariance threshold $\delta_v \leftarrow$ Eq. (10) by function $\mathbb{I}(\cdot) \leftarrow$ Eq. (9);
  Recognize the invariant/variant patterns for each node, as $\mathcal{P}_{\mathbf{e}}^I(v)$, $\mathcal{P}_{\mathbf{e}}^V(v) \leftarrow$ Eq. (11);
  Calculate task loss depending on the invariant patterns, as $\mathcal{L}_{\text{task}} \leftarrow$ Eq. (13);
  `// Environments Generalizing`
  for $j = 1, 2, \cdots, S$ **do**
    Sample items from $\mathcal{S}_{\text{ob}} \cup \mathcal{S}_{\text{ge}}$ and perform intervention for each node, as Eq. (15);
    Calculate intervention loss, as $\mathcal{L}_{\text{risk}} \leftarrow$ Eq. (14);
  end
  `// Optimize`
  Calculate the overall loss, as $\mathcal{L} \leftarrow$ Eq. (16);
  Update model parameters by minimizing $\mathcal{L}$.
end

The overall training process of our EAGLE is shown in Algorithm 1.

Computational Complexity Analysis. We analyze the computational complexity of each part in EAGLE as follows. Denote $|\mathcal{V}|$ and $|\mathcal{E}|$ as the total number of nodes and edges in each graph snapshot.

In Section 3.1, operations of the EAConv layer in EA-DGNN can be parallelized across all nodes, which is highly efficient. Thus, the computation complexity of EA-DGNN is:

$$\mathcal{O}\left(|\mathcal{E}|\sum_{l=0}^{L} d^{(l)} + \mathcal{V}\left(\sum_{l=1}^{L} d^{(l-1)}d^{(l)} + (d^{(L)})^2\right)\right), \tag{B.1}$$

where $d^{(l)}$ denotes the dimension of the l-th layer. As L is a small number, and $d^{(l)}$ is a constant, the Eq. (B.1) can be rewritten as $\mathcal{O}(|\mathcal{E}|d + |\mathcal{V}|d^2)$, where d is the universal notation of all $d^{(l)}$.

In Section 3.2, the computation complexity of the ECVAE is a compound of the encoder and decoder, with the same computation complexity as $\mathcal{O}(|\mathbf{z}|L'd)$, where $|\mathbf{z}|$ is the number of the observed environment samples, L' is the number of layers in the encoder and decoder. Also, as L' is a small number, we omit it for brevity. Thus, the computation complexity of ECVAE is $\mathcal{O}(|\mathbf{z}|d)$.

In Section 3.3, we recognize the invariant/variant patterns for all nodes by the function $\mathbb{I}(\cdot)$ in parallel, with the computation complexity $\mathcal{O}(K\log|\mathcal{V}|)$.

In Section 3.4, we perform sampling and replacing as an implementation of causal interventions. Denote $|\mathcal{E}|_p$ as the number of edges to predict and $|\mathcal{S}|$ as the size of the intervention set, which is usually set as a small constant. The spatio-temporal causal intervention mechanism owns a computation complexity compounding of sampling and replacing as $\mathcal{O}(|\mathcal{S}|d) + \mathcal{O}(|\mathcal{E}_p||\mathcal{S}|d)$ in training, and no extra computation complexity in the inference stage.

Therefore, the overall computation complexity of EAGLE is:

$$\mathcal{O}(|\mathcal{E}|d + |\mathcal{V}|d^2) + \mathcal{O}(|\mathbf{z}|d) + \mathcal{O}(K\log|\mathcal{V}|) + \mathcal{O}(|\mathcal{S}|d) + \mathcal{O}(|\mathcal{E}_p||\mathcal{S}|d). \tag{B.2}$$

In summary, EAGLE has a linear computation complexity with respect to the number of nodes and edges, which is on par with DIDA [94] and other existing dynamic GNNs. We believe that the computational complexity bottleneck of EAGLE lies in the spatio-temporal causal intervention mechanism. We further analyze the intervention efficiency in Appendix D.5.

Space Complexity Analysis. We analyze the space complexity of each part in EAGLE as follows. Denote $|\mathcal{V}|$ and $|\mathcal{E}|$ as the number of nodes and edges, respectively, K as the number of environments, T as the number of time slices, L as the number of layers in EA-DGNN, L' as the number of layers in ECVAE, d as the dimension of input node features, $d' = Kd$ as the hidden dimension of EAConv layers in EA-DGNN, d'' as the hidden dimension of the encoder and decoder networks layer of ECVAE, $\sum_{v\in\mathcal{V}}\mathrm{Var}(\mathbf{z}_v^{\mathbf{e}\prime})$ as the variance of K environment-aware representations.

Here we provide a rough analysis of EAGLE's space complexity. Note that, as the space complexity analysis of deep learning models is complicated, we omit some less important terms, such as intermediate activations, *etc.*

- storing the dynamic graph: $\mathcal{O}(KT(|\mathcal{V}| + |\mathcal{E}|))$.
- storing the node input features: $\mathcal{O}(|\mathcal{V}|KTd)$.
- the EAConv layer: $\mathcal{O}(Ld'^2)$.
- the encoder and decoder networks of ECVAE: $\mathcal{O}(L'd'')$.
- storing generated environment samples (the number set to be the same with the observed ones): $\mathcal{O}(|\mathcal{V}|KTd'')$.
- storing the states for function $\mathbb{I}(\cdot,\cdot)$: $\mathcal{O}(K\sum_{v\in\mathcal{V}}\mathrm{Var}(\mathbf{z}_v^{\mathbf{e}\prime}))$.

Then the overall space complexity of EAGLE can be roughly calculated as:

$$\mathcal{O}(KT(|\mathcal{V}| + |\mathcal{E}|)) + \mathcal{O}(|\mathcal{V}|KTd) + \mathcal{O}(Ld'^2) + \mathcal{O}(L'd'') + \mathcal{O}(|\mathcal{V}|KTd'') + \mathcal{O}(K\sum_{v\in\mathcal{V}}\mathrm{Var}(\mathbf{z}_v^{\mathbf{e}\prime})). \tag{B.3}$$

However, it is hard to intuitively draw conclusions about memory requirements from the space complexity analysis. Based on our experiments experience, EAGLE can be trained and tested under the hardware configurations (including memory requirements) listed in Appendix E.3, which is on par with the related works' requirements.

C Proofs

C.1 Proof of Proposition 1

Proposition 1. Given observed environment samples from the dynamic graph $\mathcal{G}^{1:T}$ denoted as

$$\mathbf{z} = \bigcup_{v\in\mathcal{V}} \bigcup_{k=1}^{K} \bigcup_{t=1}^{T} \{\mathbf{z}_{v,k}^{t}\} \in \mathbb{R}^{(|\mathcal{V}|\times K\times T)\times d'} \xlongequal{\text{def}} \mathcal{S}_{\text{ob}} \tag{C.1}$$

with their corresponding one-hot multi-labels $\mathbf{y}$, the environment variable $\mathbf{e}$ is drawn from the prior distribution $p_\omega(\mathbf{e} \mid \mathbf{y})$ across T time slices, and $\mathbf{z}$ is generated from the distribution $p_\omega(\mathbf{z} \mid \mathbf{y}, \mathbf{e})$. Maximizing the conditional log-likelihood $\log p_\omega(\mathbf{z} \mid \mathbf{y})$ leads to an optimal ECVAE by minimizing:

$$\mathcal{L}_{\text{ECVAE}} = \text{KL}[q_\phi(\mathbf{e} \mid \mathbf{z}, \mathbf{y}) \| p_\omega(\mathbf{e} \mid \mathbf{y})] - \frac{1}{|\mathbf{z}|} \sum_{i=1}^{|\mathbf{z}|} \log p_\omega(\mathbf{z} \mid \mathbf{y}, \mathbf{e}^{(i)}), \tag{C.2}$$

where $\text{KL}[\cdot\|\cdot]$ is the Kullback-Leibler (KL) divergence [37], $|\mathbf{z}|$ is the number of observed environment samples, $\mathbf{e}^{(i)}$ is the i-th sampling by the reparameterization trick.

Proof. The distribution distance between $q_\phi(\mathbf{e} \mid \mathbf{z}, \mathbf{y})$ and $p_\omega(\mathbf{e} \mid \mathbf{z}, \mathbf{y})$ can be calculated by the KL-divergence:

$$\begin{aligned}
\text{KL}[q_\phi(\mathbf{e} \mid \mathbf{z}, \mathbf{y}) \| p_\omega(\mathbf{e} \mid \mathbf{z}, \mathbf{y})] &= \int q_\phi(\mathbf{e} \mid \mathbf{z}, \mathbf{y}) \log \frac{q_\phi(\mathbf{e} \mid \mathbf{z}, \mathbf{y})}{p_\omega(\mathbf{e} \mid \mathbf{z}, \mathbf{y})} \, \mathrm{d}\phi \\
&= \int q_\phi(\mathbf{e} \mid \mathbf{z}, \mathbf{y}) \log \frac{q_\phi(\mathbf{e} \mid \mathbf{z}, \mathbf{y}) p_\omega(\mathbf{z} \mid \mathbf{y}) p_\omega(\mathbf{y})}{p_\omega(\mathbf{e}, \mathbf{z}, \mathbf{y})} \, \mathrm{d}\phi \\
&= \int q_\phi(\mathbf{e} \mid \mathbf{z}, \mathbf{y}) \log q_\phi(\mathbf{e} \mid \mathbf{z}, \mathbf{y}) \, \mathrm{d}\phi + \underbrace{\int q_\phi(\mathbf{e} \mid \mathbf{z}, \mathbf{y}) \log p_\omega(\mathbf{z} \mid \mathbf{y}) \, \mathrm{d}\phi}_{\log p_\omega(\mathbf{z}|\mathbf{y})} \\
&\quad + \int q_\phi(\mathbf{e} \mid \mathbf{z}, \mathbf{y}) \log p_\omega(\mathbf{y}) \, \mathrm{d}\phi - \int q_\phi(\mathbf{e} \mid \mathbf{z}, \mathbf{y}) \log p_\omega(\mathbf{e}, \mathbf{z}, \mathbf{y}) \, \mathrm{d}\phi \\
&= \log p_\omega(\mathbf{z} \mid \mathbf{y}) + \int q_\phi(\mathbf{e} \mid \mathbf{z}, \mathbf{y}) \log \frac{q_\phi(\mathbf{e} \mid \mathbf{z}, \mathbf{y})}{p_\omega(\mathbf{z} \mid \mathbf{y}, \mathbf{e}) p_\omega(\mathbf{e} \mid \mathbf{y})} \, \mathrm{d}\phi \\
&= \log p_\omega(\mathbf{z} \mid \mathbf{y}) + \mathbb{E}_{q_\phi(\mathbf{e}|\mathbf{z},\mathbf{y})}[\log q_\phi(\mathbf{e} \mid \mathbf{z}, \mathbf{y}) - \log p_\omega(\mathbf{e}, \mathbf{z} \mid \mathbf{y})] \\
&= \log p_\omega(\mathbf{z} \mid \mathbf{y}) - \mathbb{E}_{q_\phi(\mathbf{e}|\mathbf{z},\mathbf{y})}[-\log q_\phi(\mathbf{e} \mid \mathbf{z}, \mathbf{y}) + \log p_\omega(\mathbf{e}, \mathbf{z} \mid \mathbf{y})].
\end{aligned} \tag{C.3}$$

Thus the conditional log-likelihood $\log p_\omega(\mathbf{z} \mid \mathbf{y})$ can be rewritten as:

$$\log p_\omega(\mathbf{z} \mid \mathbf{y}) = \text{KL}[q_\phi(\mathbf{e} \mid \mathbf{z}, \mathbf{y}) \| p_\omega(\mathbf{e} \mid \mathbf{z}, \mathbf{y})] + \mathbb{E}_{q_\phi(\mathbf{e}|\mathbf{z},\mathbf{y})}[-\log q_\phi(\mathbf{e} \mid \mathbf{z}, \mathbf{y}) + \log p_\omega(\mathbf{e}, \mathbf{z} \mid \mathbf{y})]. \tag{C.4}$$

Since this KL-divergence is non-negative, we then provide an Evidence Lower Bound (ELBO) for $\log p_\omega(\mathbf{y} \mid \mathbf{z})$:

$$\begin{aligned}
\log p_\omega(\mathbf{z} \mid \mathbf{y}) &\geq \mathbb{E}_{q_\phi(\mathbf{e}|\mathbf{z},\mathbf{y})}[-\log q_\phi(\mathbf{e} \mid \mathbf{z}, \mathbf{y}) + \log p_\omega(\mathbf{e}, \mathbf{z} \mid \mathbf{y})] \\
&= \mathbb{E}_{q_\phi(\mathbf{e}|\mathbf{z},\mathbf{y})}[-\log q_\phi(\mathbf{e} \mid \mathbf{z}, \mathbf{y}) + \log p_\omega(\mathbf{e} \mid \mathbf{y})] + \mathbb{E}_{q_\phi(\mathbf{e}|\mathbf{z},\mathbf{y})}[\log p_\omega(\mathbf{z} \mid \mathbf{y}, \mathbf{e})] \\
&= -\text{KL}[q_\phi(\mathbf{e} \mid \mathbf{z}, \mathbf{y}) \| p_\omega(\mathbf{e} \mid \mathbf{y})] + \mathbb{E}_{q_\phi(\mathbf{e}|\mathbf{z},\mathbf{y})}[\log p_\omega(\mathbf{z} \mid \mathbf{y}, \mathbf{e})].
\end{aligned} \tag{C.5}$$

We can maximize $\log p_\omega(\mathbf{z} \mid \mathbf{y})$ by maximizing the ELBO, or minimizing:

$$\mathcal{L}_{\text{ECVAE}} = -\text{ELBO} = \text{KL}[q_\phi(\mathbf{e} \mid \mathbf{z}, \mathbf{y}) \| p_\omega(\mathbf{e} \mid \mathbf{y})] - \mathbb{E}_{q_\phi(\mathbf{e}|\mathbf{z},\mathbf{y})}[\log p_\omega(\mathbf{z} \mid \mathbf{y}, \mathbf{e})]. \tag{C.6}$$

While the second term in $\mathcal{L}_{\text{ECVAE}}$ is the maximum likelihood estimation, which is infeasible to calculate directly under the expectation of the latent environment variable $\mathbf{e} \sim p_\phi(\mathbf{e} \mid \mathbf{z}, \mathbf{y})$ across T time slices. Inspired by Markov Chain Monte Carlo (MCMC) sampling [23], it can be estimated as:

$$\mathcal{L}_{\text{ECVAE}} = \text{KL}[q_\phi(\mathbf{e} \mid \mathbf{z}, \mathbf{y}) \| p_\omega(\mathbf{e} \mid \mathbf{y})] - \frac{1}{|\mathbf{z}|} \sum_{i=1}^{|\mathbf{z}|} \log p_\omega(\mathbf{z} \mid \mathbf{y}, \mathbf{e}^{(i)}). \tag{C.7}$$

In implementations, we assume $q_\phi(\mathbf{e} \mid \mathbf{z}, \mathbf{y})$ and $p_\omega(\mathbf{e} \mid \mathbf{y})$ follow the multivariate normal distribution $\mathcal{N}(\boldsymbol{\mu}; \boldsymbol{\sigma})$ parameterized by $\boldsymbol{\mu}$ and $\boldsymbol{\sigma}$, so that the KL-divergence can be easily calculated. In order to optimize the ECVAE by back-propagation, we utilize a reparameterization trick: $\mathbf{e}^{(i)} = e_\omega(\mathbf{z}, \mathbf{y}, \epsilon^{(i)})$, where $\epsilon^{(i)} \sim \mathcal{N}(\mathbf{0}; \mathbf{I})$. Here $e_\omega(\cdot, \cdot, \cdot)$ is some vector-valued functions parameterized by ϕ. □

C.2 Proof of Proposition 2

Proposition 2 (A Solution for $\mathbb{I}^\star(\cdot)$)**.** Denote $\mathbf{z}_v^{\mathbf{e}\prime} = [\mathbf{z}'_{v,1}, \mathbf{z}'_{v,2}, \cdots, \mathbf{z}'_{v,K}]$, where $\mathbf{z}'_{v,k} = \bigcup_{t=1}^{T} \mathbf{z}_{v,k}^t$. Let $\mathrm{Var}(\mathbf{z}_v^{\mathbf{e}\prime}) \in \mathbb{R}^K$ represents the variance of K environment-aware representations. The Boolean function $\mathbb{I}(\cdot)$ is a solution for $\mathbb{I}^\star(\cdot)$ with the following state update equation:

$$\mathbb{I}(i,j) = \begin{cases} \mathbb{I}(i-1,j) \vee \mathbb{I}(i-1, j - \mathrm{Var}(\mathbf{z}_v^{\mathbf{e}\prime})[i-1]), & j \geq \mathrm{Var}(\mathbf{z}_v^{\mathbf{e}\prime})[i-1] \\ \mathbb{I}(i-1,j), & \text{otherwise} \end{cases}, \tag{C.8}$$

$\mathbb{I}(i,j)$ indicates whether it is feasible to select from the first i elements in $\mathrm{Var}(\mathbf{z}_v^{\mathbf{e}\prime})$ so that their sum is j. Traversing j in reverse order from $\lfloor \sum \mathrm{Var}(\mathbf{z}_v^{\mathbf{e}\prime})/2 \rfloor$ until satisfying $\mathbb{I}(K,j)$ is True, we reach:

$$\delta_v = \sum \mathrm{Var}(\mathbf{z}_v^{\mathbf{e}\prime}) - 2j, \tag{C.9}$$

$$\mathcal{P}_{\mathbf{e}}^I(v) = \left\{ \mathbf{e}_k \mid \mathrm{Var}(\mathbf{z}_v^{\mathbf{e}\prime})[k] \leq \frac{1}{K} \sum \mathrm{Var}(\mathbf{z}_v^{\mathbf{e}\prime}) - \frac{\delta_v}{2} \right\}, \quad \mathcal{P}_{\mathbf{e}}^V(v) = \overline{\mathcal{P}_{\mathbf{e}}^I(v)}, \tag{C.10}$$

where δ_v is the optimal spatio-temporal invariance threshold of node v.

Proof. In order to prove the boolean function $\mathbb{I}(\cdot)$ is a solution for $\mathbb{I}^\star(\cdot)$ in Assumption 1, the problem $\mathbb{I}(\cdot)$ solves should satisfies: **(a) Optimal substructure**; **(b) Non-aftereffect property**; **(c) Overlapping sub-problems**.

Next, we prove the above three conditions are valid.

(a) Optimal substructure. It is said that the problem has the optimal substructure property when the optimal solution of the problem covers the optimal solutions of its subproblems. Now we prove the optimal solution of determining the spatio-temporal invariant patterns $\mathcal{P}_{\mathbf{e}}^I(v)$ for node v is constructed from the optimal solutions of the sub-problems with the bottom-up approach by using the optimal substructure property of the problem.

As $\mathbb{I}(i,j)$ indicates whether it is feasible to select some elements from the first i elements in $\mathrm{Var}(\mathbf{z}_v^{\mathbf{e}\prime})$ so that their sum is j, $\sum \mathrm{Var}(\mathbf{z}_v^{\mathbf{e}\prime})$ means the sum of elements in $\mathrm{Var}(\mathbf{z}_v^{\mathbf{e}\prime})$, the target of the problem is to find δ_v that denotes the optimal threshold for invariance of node v. We reduce this problem by dividing $\mathrm{Var}(\mathbf{z}_v^{\mathbf{e}\prime})$ into two subsets $\mathrm{Var}(\mathbf{z}_v^{\mathbf{e}\prime})_I$ and $\mathrm{Var}(\mathbf{z}_v^{\mathbf{e}\prime})_V$, where δ_v represents the value when the difference between the sum of two subsets is the smallest, *i.e.*,

$$\delta_v = \min \left(\sum \mathrm{Var}(\mathbf{z}_v^{\mathbf{e}\prime}) - 2j \right), \quad \text{where} \quad \mathbb{I}(K,j) == \text{True}. \tag{C.11}$$

Let $\mathbb{I}_I(i,j)$ and $\mathbb{I}_V(i,j)$ represent whether it is feasible to select some elements from the first i elements in $\mathrm{Var}(\mathbf{z}_v^{\mathbf{e}\prime})_I$ and $\mathrm{Var}(\mathbf{z}_v^{\mathbf{e}\prime})_V$ respectively, so that their sum is j. Suppose the sum of $\mathrm{Var}(\mathbf{z}_v^{\mathbf{e}\prime})_I$ and $\mathrm{Var}(\mathbf{z}_v^{\mathbf{e}\prime})_V$ are $\sum(\mathrm{Var}(\mathbf{z}_v^{\mathbf{e}\prime})_I)$ and $\sum(\mathrm{Var}(\mathbf{z}_v^{\mathbf{e}\prime})_V)$, we have:

$$\sum(\mathrm{Var}(\mathbf{z}_v^{\mathbf{e}\prime})_I) + \sum(\mathrm{Var}(\mathbf{z}_v^{\mathbf{e}\prime})_V) = \sum \mathrm{Var}(\mathbf{z}_v^{\mathbf{e}\prime}). \tag{C.12}$$

Then, the target of the original problem is transformed into finding an optimal solution for i and j, satisfying:

$$\begin{cases} \mathbb{I}_I(i,j) == \text{True}, \\ \mathbb{I}_V(K-i, \sum(\mathrm{Var}(\mathbf{z}_v^{\mathbf{e}\prime})_I) - j) == \text{True}, \end{cases} \tag{C.13}$$

$$\textit{s.t.} \ \min \left(\sum(\mathrm{Var}(\mathbf{z}_v^{\mathbf{e}\prime})_I) - j - \left(\sum(\mathrm{Var}(\mathbf{z}_v^{\mathbf{e}\prime})_V) - \left(\sum(\mathrm{Var}(\mathbf{z}_v^{\mathbf{e}\prime})_I) - j \right) \right) \right). \tag{C.14}$$

According to the definition of $\mathbb{I}(i,j)$, we can draw a conclusion the $\mathbb{I}_I(i,j)$ and $\mathbb{I}_V(i,j)$ both are the subproblems of the original problem, which similarly target at figuring out whether it is feasible to select some elements from the first i elements that satisfy their sum is j. So, function $\mathbb{I}_I(i,j)$ and

$\mathbb{I}_V(i,j)$ is the same with $\mathbb{I}(i,j)$ in Eq. (C.8). Assuming that when the difference in the subsets is maximized, $\mathbb{I}_I(i,j)$ and $\mathbb{I}_V(i,j)$ return j_I and j_V, respectively, that satisfy:

$$\begin{cases} \mathbb{I}_I(i, j_I) == \text{True}, \\ \mathbb{I}_V(K-i, j_V) == \text{True}. \end{cases} \tag{C.15}$$

We have:

$$\begin{cases} \sum(\text{Var}(\mathbf{z}_v^{\mathbf{e}\prime})_I) - j_I = \delta_I, & \mathbb{I}_I(i, j_I) == \text{True}, \\ \sum(\text{Var}(\mathbf{z}_v^{\mathbf{e}\prime})_V) - j_V = \delta_V, & \mathbb{I}_V(K-i, \sum(\text{Var}(\mathbf{z}_v^{\mathbf{e}\prime})_I) - j_I) == \text{True}. \end{cases} \tag{C.16}$$

As $\mathbb{I}_I(i, j_I)$ and $\mathbb{I}_V(K-i, \sum(\text{Var}(\mathbf{z}_v^{\mathbf{e}\prime})_I) - j_I)$ are both the optimal solutions, so we reach:

$$|\delta_I - \delta_V| = \left| \sum(\text{Var}(\mathbf{z}_v^{\mathbf{e}\prime})_I) - j_I - \left(\sum(\text{Var}(\mathbf{z}_v^{\mathbf{e}\prime})_V) - j_V \right) \right| \leq \delta_v. \tag{C.17}$$

The optimal substructure property is proven.

(b) Non-aftereffect property. This property implies that once the state of a certain stage is determined by $\mathbb{I}(\cdot)$, it is not affected by future decision-making. In other words, the subsequent process will not affect the previous state, but only be related to the current state. Eq. (C.8) implies that, when $j \geq \text{Var}(\mathbf{z}_v^{\mathbf{e}\prime})[i-1]$, the state is decided by previous state $\mathbb{I}(i-1, j)$ or $\mathbb{I}(i-1, j - \text{Var}(\mathbf{z}_v^{\mathbf{e}\prime})[i-1])$; accordingly, when $j < \text{Var}(\mathbf{z}_v^{\mathbf{e}\prime})[i-1]$, the state is solely decided by previous state $\mathbb{I}(i-1, j)$. All state transition processes are based on historical states and executed in a one-way transition mode, meeting the requirements of the non-aftereffect property. Generally speaking, the non-aftereffect property is a relaxation condition, that is, as long as the properties of the optimal substructure property are satisfied, the non-aftereffect property will be basically satisfied.

(c) Overlapping sub-problems. $\mathbb{I}(\cdot)$ solve the problem from top to bottom in a recursive way, each sub-problem is not always a new problem, but a large number of repeated sub-problems, that is, when different decision sequences reach a certain stage, they will generate duplicate problems. When figuring out $\mathbb{I}(\cdot)$, we consider two situations:

- Not select the i-th element in $\text{Var}(\mathbf{z}_v^{\mathbf{e}\prime})$, *i.e.*, $\mathbb{I}(i,j) = \mathbb{I}(i-1, j)$;
- Select the i-th element in $\text{Var}(\mathbf{z}_v^{\mathbf{e}\prime})$, *i.e.*, $\mathbb{I}(i,j) = \mathbb{I}(i-1, j - \text{Var}(\mathbf{z}_v^{\mathbf{e}\prime})[i-1])$.

As we can observe, we need the solution of the sub-problem $\mathbb{I}(i-1, j)$ and $\mathbb{I}(i-1, j-\text{Var}(\mathbf{z}_v^{\mathbf{e}\prime})[i-1])$ when figuring out $\mathbb{I}(i,j)$, which are already calculated by $\mathbb{I}(i-1, \cdot)$. So we can prove that the problem $\mathbb{I}(\cdot)$ solved has overlapping sub-problems.

We then have proven the function $\mathbb{I}(\cdot)$ is a solution for the function $\mathbb{I}^\star(\cdot)$ in Assumption 1, from which we can obtain the optimal spatio-temporal invariance threshold δ_v of node v. Then the spatio-temporal invariant/variant patterns for node v can be exploited by Eq. (C.10), and their unions constitute the overall $\mathcal{P}_{\mathbf{e}}^I$ and $\mathcal{P}_{\mathbf{e}}^V$. We conclude the proof for Proposition 2. □

C.3 Proof of Proposition 3

Proposition 3 (Achievable Assumption)**.** Minimizing Eq. (12) can encourage the model to satisfy the Invariance Property and Sufficient Condition in Assumption 1.

Proof. We first propose the following lemma to rewrite the Sufficient Condition and the Invariance Property in Assumption 1 using the information theory [43].

Lemma 1 (Mutual Information Equivalence)**.** The Invariance Property and Sufficient Condition in Assumption 1 can be equivalently represented with the Mutual Information $I(\cdot;\cdot)$:

(a) Invariance Property: $p(\mathbf{Y}^T \mid \mathcal{P}_{\mathbf{e}}^I, \mathbf{e}) = p(\mathbf{Y}^T \mid \mathcal{P}_{\mathbf{e}}^I) \Leftrightarrow I(\mathbf{Y}^T; \mathbf{e} \mid \mathcal{P}_{\mathbf{e}}^I) = 0$;

(b) Sufficient Condition: $\mathbf{Y}^T \perp\!\!\!\perp \mathcal{P}_{\mathbf{e}}^V \mid \mathcal{P}_{\mathbf{e}}^I \Leftrightarrow I(\mathbf{Y}^T; \mathcal{P}_{\mathbf{e}}^I)$ is maximized.

Proof. We prove Lemma 1 by respectively proving the above two conditions are valid.

(a) Invariance Property. According to the definition of the Mutual Information, we can easily get the following equation:

$$I(\mathbf{Y}^T; \mathbf{e} \mid \mathcal{P}_{\mathbf{e}}^I) = \mathrm{KL}\left[p(\mathbf{Y}^T \mid \mathbf{e}, \mathcal{P}_{\mathbf{e}}^I) \parallel p(\mathbf{Y}^T \mid \mathcal{P}_{\mathbf{e}}^I)\right] = 0, \tag{C.18}$$

where $\mathrm{KL}[\cdot\|\cdot]$ is the Kullback-Leibler (KL) divergence [37]. Thus we have proved the equivalence in Invariance Property.

(b) Sufficient Condition. We demonstrate sufficiency and necessity through the following two steps.

First, we prove that for $\mathbf{Y}^T$, $\mathcal{P}_{\mathbf{e}}^I$ and ϵ satisfying $\mathbf{Y}^T = g(\mathbf{Z}_I^{1:T}) + \epsilon$ would also satisfy $\mathcal{P}_{\mathbf{e}}^I = \arg\max_{\mathcal{P}_{\mathbf{e}}^I} I(\mathbf{Y}^T; \mathcal{P}_{\mathbf{e}}^I)$. We perform proving by contradiction. Suppose $\mathcal{P}_{\mathbf{e}}^I \neq \arg\max_{\mathcal{P}_{\mathbf{e}}^I} I(\mathbf{Y}^T; \mathcal{P}_{\mathbf{e}}^I)$ and there exists $\mathcal{P}_{\mathbf{e}}^{I\prime} = \arg\max_{\mathcal{P}_{\mathbf{e}}^I}$ where $\mathcal{P}_{\mathbf{e}}^{I\prime} \neq \mathcal{P}_{\mathbf{e}}^I$. We can always find a mapping function $\mathcal{M}$ so that $\mathcal{P}_{\mathbf{e}}^{I\prime} = \mathcal{M}(\mathcal{P}_{\mathbf{e}}^I, \pi)$ where π is a random variable. Then we reach:

$$I(\mathbf{Y}^T; \mathcal{P}_{\mathbf{e}}^{I\prime}) = I(\mathbf{Y}^T; \mathcal{P}_{\mathbf{e}}^I, \pi) = I(g(\mathbf{Z}_I^{1:T}); \mathcal{P}_{\mathbf{e}}^I, \pi) = I(g(\mathbf{Z}_I^{1:T}); \mathcal{P}_{\mathbf{e}}^I) = I(\mathbf{Y}^T; \mathcal{P}_{\mathbf{e}}^I), \tag{C.19}$$

which leads to a contradiction.

Next, we prove that for $\mathbf{Y}^T$, $\mathcal{P}_{\mathbf{e}}^I$ and ϵ satisfying $\mathcal{P}_{\mathbf{e}}^I = \arg\max_{\mathcal{P}_{\mathbf{e}}^I} I(\mathbf{Y}^T; \mathcal{P}_{\mathbf{e}}^I)$ would also satisfy $\mathbf{Y}^T = g(\mathbf{Z}_I^{1:T}) + \epsilon$. We also perform proving by contradiction. Suppose that $\mathbf{Y}^T \neq g(\mathbf{Z}_I^{1:T}) + \epsilon$ and $\mathbf{Y}^T = g(\mathbf{Z}_{I'}^{1:T}) + \epsilon$ where $\mathcal{P}_{\mathbf{e}}^{I\prime} \neq \mathcal{P}_{\mathbf{e}}^I$. We then have the following inequality:

$$I(g(\mathbf{Z}_{I'}^{1:T}); \mathcal{P}_{\mathbf{e}}^I) \leq I(g(\mathbf{Z}_{I'}^{1:T}); \mathcal{P}_{\mathbf{e}}^{I\prime}), \tag{C.20}$$

from which we can obtain that $\mathcal{P}_{\mathbf{e}}^{I\prime} = \arg\max_{\mathcal{P}_{\mathbf{e}}^I} I(\mathbf{Y}^T; \mathcal{P}_{\mathbf{e}}^I)$, leading to a contradiction. □

Now, we prove Proposition 3 in the following two perspectives.

First, we prove that minimizing the expectation term ($\mathcal{L}_{\text{task}}$) in Eq. (12) can enforce the model to satisfy the Sufficient Condition in Assumption 1 (note that we omit the subscript $\mathcal{P}_{\mathbf{e}}^I$ in $\mathbf{Z}_I^{1:T}$ for brevity in the rest of this subsection if there are no special declarations).

From the SCM model in Figure 1(b), we can analyze that $\max_{q(\mathbf{Z}^{1:T}|\mathbf{G}^{1:T})} I(\mathbf{Y}^T; \mathbf{Z}^{1:T})$ is equivalent to $\min_{q(\mathbf{Z}^{1:T}|\mathbf{G}^{1:T})} I(\mathbf{Y}^T; \mathbf{G}^{1:T} \mid \mathbf{Z}^{1:T})$, as we filter out the spurious correlations that contain in the dependencies between $\mathbf{Y}^T$ and $\mathbf{G}^{1:T}$. Treating $q(\mathbf{Z}^{1:T} \mid \mathbf{G}^{1:T})$ as the variational distribution, we have the following upper bound:

$$\begin{aligned}
I(\mathbf{Y}^T; \mathbf{G}^{1:T} \mid \mathbf{Z}^{1:T}) &= \mathrm{KL}\left[p(\mathbf{Y}^T \mid \mathbf{G}^{1:T}, \mathbf{e}) \parallel p(\mathbf{Y}^T \mid \mathbf{Z}^{1:T}, \mathbf{e})\right] \\
&= \mathrm{KL}\left[p(\mathbf{Y}^T \mid \mathbf{G}^{1:T}, \mathbf{e}) \parallel q(\mathbf{Y}^T \mid \mathbf{Z}^{1:T})\right] \\
&\quad - \mathrm{KL}\left[p(\mathbf{Y}^T \mid \mathbf{Z}^{1:T}, \mathbf{e}) \parallel q(\mathbf{Y}^T \mid \mathbf{Z}^{1:T})\right] \\
&\leq \mathrm{KL}\left[p(\mathbf{Y}^T \mid \mathbf{G}^{1:T}, \mathbf{e}) \parallel q(\mathbf{Y}^T \mid \mathbf{Z}^{1:T})\right] \\
&\leq \min_{q(\mathbf{Y}^T|\mathbf{Z}^{1:T})} \mathrm{KL}\left[p(\mathbf{Y}^T \mid \mathbf{G}^{1:T}, \mathbf{e}) \parallel q(\mathbf{Y}^T \mid \mathbf{Z}^{1:T})\right].
\end{aligned} \tag{C.21}$$

In addition, we have:

$$\begin{aligned}
&\mathrm{KL}\left[p(\mathbf{Y}^T \mid \mathbf{G}^{1:T}, \mathbf{e}) \parallel q(\mathbf{Y}^T \mid \mathbf{Z}^{1:T})\right] \\
&= \mathbb{E}_{\mathbf{e}} \mathbb{E}_{(\mathcal{G}^{1:T}, Y^T) \sim p(\mathbf{G}^{1:T}, \mathbf{Y}^T|\mathbf{e})} \mathbb{E}_{\mathbf{Z}^{1:T} \sim q(\mathbf{Z}^{1:T}|\mathbf{G}^{1:T}=\mathcal{G}^{1:T})} \left[\log \frac{p(\mathbf{Y}^T = Y^T \mid \mathbf{G}^{1:T} = \mathcal{G}^{1:T}, \mathbf{e})}{q(\mathbf{Y}^T = Y^T \mid \mathbf{Z}^{1:T})}\right] \\
&\leq \mathbb{E}_{\mathbf{e}} \mathbb{E}_{(\mathcal{G}^{1:T}, Y^T) \sim p(\mathbf{G}^{1:T}, \mathbf{Y}^T|\mathbf{e})} \left[\log \frac{(\mathbf{Y}^T = Y^T \mid \mathbf{G}^{1:T} = \mathcal{G}^{1:T}, \mathbf{e})}{\mathbb{E}_{\mathbf{Z}^{1:T} \sim q(\mathbf{Z}^{1:T}|\mathbf{G}^{1:T}=\mathcal{G}^{1:T})} \left[q(\mathbf{Y}^T = Y^T \mid \mathbf{Z}^{1:T})\right]}\right].
\end{aligned} \tag{C.22}$$

The inequality in Eq. (C.22) is derived from Jensen's Inequality [34] and [86], while the EA-DGNN $w(\cdot)$ ensures $q(\mathbf{Z}^{1:T} \mid \mathbf{G}^{1:T})$ is a Dirac delta distribution (δ-distribution). Then we reach:

$$\begin{aligned}
&\min_{q(\mathbf{Y}^T|\mathbf{Z}^{1:T})} \mathrm{KL}\left[p(\mathbf{Y}^T \mid \mathbf{G}^{1:T}, \mathbf{e}) \parallel q(\mathbf{Y}^T \mid \mathbf{Z}^{1:T})\right] \\
&\Leftrightarrow \min_{\boldsymbol{\theta}} \mathbb{E}_{\mathbf{e} \sim q_\phi(\mathbf{e}), (\mathcal{G}^{1:T}, Y^T) \sim p(\mathbf{G}^{1:T}, \mathbf{Y}^T|\mathbf{e})} \left[\ell\left(g(\mathbf{Z}_I^{1:T}), Y^T\right)\right].
\end{aligned} \tag{C.23}$$

We thus have proven that, minimizing the expectation term ($\mathcal{L}_{\text{task}}$) in Eq. (12) is to minimize the upper bound of $I(\mathbf{Y}^T; \mathbf{G}^{1:T} \mid \mathbf{Z}^{1:T})$ (maximize the lower bound of $\max_{q(\mathbf{Z}^{1:T}|\mathbf{G}^{1:T})} I(\mathbf{Y}^T; \mathbf{Z}^{1:T})$), which leads to maximizing $I(\mathbf{Y}^T; \mathcal{P}_{\mathbf{e}}^I)$. This helps enforce the model to satisfy the Sufficient Condition.

Then, we prove that minimizing the variance term ($\mathcal{L}_{\text{risk}}$) in Eq. (12) can enforce the model to satisfy the Invariance Property in Assumption 1.

We have:

$$\begin{aligned} I(\mathbf{Y}^T; \mathbf{e} \mid \mathbf{Z}^{1:T}) &= \mathrm{KL}\left[p(\mathbf{Y}^T \mid \mathbf{Z}^{1:T}, \mathbf{e}) \parallel p(\mathbf{Y}^T \mid \mathbf{Z}^{1:T})\right] \\ &= \mathrm{KL}\left[p(\mathbf{Y}^T \mid \mathbf{Z}^{1:T}, \mathbf{e}) \parallel \mathbb{E}_{\mathbf{e}}\left[p(\mathbf{Y}^T \mid \mathbf{Z}^{1:T}, \mathbf{e})\right]\right] \\ &= \mathrm{KL}\left[q(\mathbf{Y}^T \mid \mathbf{Z}^{1:T}) \parallel \mathbb{E}_{\mathbf{e}} q(\mathbf{Y}^T \mid \mathbf{Z}^{1:T})\right] \\ &\quad - \mathrm{KL}\left[q(\mathbf{Y}^T \mid \mathbf{Z}^{1:T}) \parallel p(\mathbf{Y}^T \mid \mathbf{Z}^{1:T}, \mathbf{e})\right] \\ &\quad - \mathrm{KL}\left[\mathbb{E}_{\mathbf{e}}\left[p(\mathbf{Y}^T \mid \mathbf{Z}^{1:T}, \mathbf{e})\right] \parallel \mathbb{E}_{\mathbf{e}}\left[q(\mathbf{Y}^T \mid \mathbf{Z}^{1:T})\right]\right] \\ &\leq \mathrm{KL}\left[q(\mathbf{Y}^T \mid \mathbf{Z}^{1:T}) \parallel \mathbb{E}_{\mathbf{e}} q(\mathbf{Y}^T \mid \mathbf{Z}^{1:T})\right] \\ &\leq \min_{q(\mathbf{Y}^T|\mathbf{Z}^{1:T})} \mathrm{KL}\left[q(\mathbf{Y}^T \mid \mathbf{Z}^{1:T}) \parallel \mathbb{E}_{\mathbf{e}} q(\mathbf{Y}^T \mid \mathbf{Z}^{1:T})\right]. \end{aligned} \tag{C.24}$$

In addition, we have:

$$\begin{aligned} &\mathrm{KL}\left[q(\mathbf{Y}^T \mid \mathbf{Z}^{1:T}) \parallel \mathbb{E}_{\mathbf{e}} q(\mathbf{Y}^T \mid \mathbf{Z}^{1:T})\right] \\ &= \mathbb{E}_{\mathbf{e}} \mathbb{E}_{(\mathcal{G}^{1:T}, Y^T) \sim p(\mathbf{G}^{1:T}, \mathbf{Y}^T|\mathbf{e})} \mathbb{E}_{\mathbf{Z}^{1:T} \sim q(\mathbf{Z}^{1:T}|\mathbf{G}^{1:T} = \mathcal{G}^{1:T})} \left[\log \frac{q(\mathbf{Y}^T = Y^T \mid \mathbf{Z}^{1:T})}{\mathbb{E}_{\mathbf{e}} q(\mathbf{Y}^T = Y^T \mid \mathbf{Z}^{1:T})}\right]. \end{aligned} \tag{C.25}$$

Derived from Jensen's Inequality, the upper bound for $\mathrm{KL}\left[q(\mathbf{Y}^T \mid \mathbf{Z}^{1:T}) \parallel \mathbb{E}_{\mathbf{e}} q(\mathbf{Y}^T \mid \mathbf{Z}^{1:T})\right]$ is:

$$\begin{aligned} &\mathrm{KL}\left[q(\mathbf{Y}^T \mid \mathbf{Z}^{1:T}) \parallel \mathbb{E}_{\mathbf{e}} q(\mathbf{Y}^T \mid \mathbf{Z}^{1:T})\right] \\ &\leq \mathbb{E}_{\mathbf{e}}\left[\left|\ell\left(f_{\boldsymbol{\theta}}\left(\mathcal{G}^{1:T}\right), Y^T\right) - \mathbb{E}_{\mathbf{e}}\left[\ell\left(f_{\boldsymbol{\theta}}\left(\mathcal{G}^{1:T}\right), Y^T\right)\right]\right|\right]. \end{aligned} \tag{C.26}$$

Finally, we reach:

$$\begin{aligned} &\min_{q(\mathbf{Y}^T|\mathbf{Z}^{1:T})} \mathrm{KL}\left[q(\mathbf{Y}^T \mid \mathbf{Z}^{1:T}) \parallel \mathbb{E}_{\mathbf{e}} q(\mathbf{Y}^T \mid \mathbf{Z}^{1:T})\right] \\ &\Leftrightarrow \min_{\boldsymbol{\theta}} \mathrm{Var}_{s \in \mathcal{S}}\left\{\mathbb{E}_{\mathbf{e} \sim q_\phi(\mathbf{e}), (\mathcal{G}^{1:T}, Y^T) \sim p(\mathbf{G}^{1:T}, \mathbf{Y}^T|\mathbf{e})}\left[\ell\left(f_{\boldsymbol{\theta}}\left(\mathcal{G}^{1:T}\right), Y^T \mid \mathrm{do}(\mathbf{Z}_V^{1:T} = s)\right)\right]\right\}. \end{aligned} \tag{C.27}$$

We thus have proven that, minimizing the variance term ($\mathcal{L}_{\text{risk}}$) in Eq. (12) is to minimize the upper bound of $I(\mathbf{Y}^T; \mathbf{e} \mid \mathbf{Z}^{1:T})$, which leads to minimizing $I(\mathbf{Y}^T; \mathbf{e} \mid \mathcal{P}_{\mathbf{e}}^I)$. This helps enforce the model to satisfy the Invariance Property.

We conclude the proof for Proposition 3. □

C.4 Proof of Proposition 4

Proposition 4 (Equivalent Optimization)**.** Optimizing Eq. (12) is equivalent to minimizing the upper bound of the OOD generalization error in Eq. (2).

Proof. As we defined in Eq. (2), the generation of dynamic graph data $(\mathcal{G}^{1:T}, Y^T)$ is drawn from the distribution $p(\mathbf{G}^{1:T}, \mathbf{Y}^T \mid \mathbf{e})$, while the difference of $\mathbf{e}$ during training and testing causes the out-of-distribution shifts. Let $q(\mathbf{Y}^T \mid \mathbf{G}^{1:T})$ be the inferred variational distribution of the ground-truth distribution $p(\mathbf{Y}^T \mid \mathbf{G}^{1:T}, \mathbf{e})$, then the OOD generalization error can be measured by the KL-divergence of the two distributions:

$$\begin{aligned} &\mathrm{KL}\left[p(\mathbf{Y}^T \mid \mathbf{G}^{1:T}, \mathbf{e}) \parallel q(\mathbf{Y}^T \mid \mathbf{G}^{1:T})\right] \\ &= \mathbb{E}_{\mathbf{e}} \mathbb{E}_{(\mathcal{G}^{1:T}, Y^T) \sim p(\mathbf{G}^{1:T}, \mathbf{Y}^T|\mathbf{e})}\left[\log \frac{p(\mathbf{Y}^T = Y^T \mid \mathbf{G}^{1:T} = \mathcal{G}^{1:T}, \mathbf{e})}{q(\mathbf{Y}^T = Y^T \mid \mathbf{G}^{1:T} = \mathcal{G}^{1:T})}\right]. \end{aligned} \tag{C.28}$$

Inspired by [19, 86], we apply an information-theoretic approach to our scenarios. First, we propose the following lemma in order to rewrite the OOD generalization error.

Lemma 2 (OOD Generalization Upper Bound)**.** The OOD generalization error is upper bounded by:

$$\mathrm{KL}\left[p(\mathbf{Y}^T \mid \mathbf{G}^{1:T}, \mathbf{e}) \parallel q(\mathbf{Y}^T \mid \mathbf{G}^{1:T})\right] \leq \mathrm{KL}\left[p(\mathbf{Y}^T \mid \mathbf{G}^{1:T}, \mathbf{e}) \parallel q(\mathbf{Y}^T \mid \mathbf{Z}^{1:T})\right], \tag{C.29}$$

where $q(\mathbf{Y}^T \mid \mathbf{Z}^{1:T})$ can be seen as the inferred variational distribution of the edge predictor.

Proof. We prove Lemma 2 by continue investigating on Eq. (C.28):

$$\begin{aligned}
&\mathrm{KL}\left[p(\mathbf{Y}^T \mid \mathbf{G}^{1:T}, \mathbf{e}) \parallel q(\mathbf{Y}^T \mid \mathbf{G}^{1:T})\right] \\
&= \mathbb{E}_{\mathbf{e}} \mathbb{E}_{(\mathcal{G}^{1:T}, Y^T) \sim p(\mathbf{G}^{1:T}, \mathbf{Y}^T \mid \mathbf{e})} \left[\log \frac{p(\mathbf{Y}^T = Y^T \mid \mathbf{G}^{1:T} = \mathcal{G}^{1:T}, \mathbf{e})}{q(\mathbf{Y}^T = Y^T \mid \mathbf{G}^{1:T} = \mathcal{G}^{1:T})}\right] \\
&= \mathbb{E}_{\mathbf{e}} \mathbb{E}_{(\mathcal{G}^{1:T}, Y^T) \sim p(\mathbf{G}^{1:T}, \mathbf{Y}^T \mid \mathbf{e})} \left[\log \frac{p(\mathbf{Y}^T = Y^T \mid \mathbf{G}^{1:T} = \mathcal{G}^{1:T}, \mathbf{e})}{\mathbb{E}_{\mathbf{Z}^{1:T} \sim q(\mathbf{Z}^{1:T} \mid \mathbf{G}^{1:T} = \mathcal{G}^{1:T})}\left[q(\mathbf{Y}^T = Y^T \mid \mathbf{Z}^{1:T})\right]}\right] \\
&\leq \mathbb{E}_{\mathbf{e}} \mathbb{E}_{(\mathcal{G}^{1:T}, Y^T) \sim p(\mathbf{G}^{1:T}, \mathbf{Y}^T \mid \mathbf{e})} \mathbb{E}_{\mathbf{Z}^{1:T} \sim q(\mathbf{Z}^{1:T} \mid \mathbf{G}^{1:T} = \mathcal{G}^{1:T})} \left[\log \frac{p(\mathbf{Y}^T = Y^T \mid \mathbf{G}^{1:T} = \mathcal{G}^{1:T}, \mathbf{e})}{q(\mathbf{Y}^T = Y^T \mid \mathbf{Z}^{1:T})}\right] \\
&= \mathrm{KL}\left[p(\mathbf{Y}^T \mid \mathbf{G}^{1:T}, \mathbf{e}) \parallel q(\mathbf{Y}^T \mid \mathbf{Z}^{1:T})\right]. \quad \text{(upper bound for OOD generalization error)}
\end{aligned} \tag{C.30}$$

Again, the inequality in Eq. (C.22) is derived from Jensen's Inequality, while the EA-DGNN $w(\cdot)$ ensures $q(\mathbf{Z}^{1:T} \mid \mathbf{G}^{1:T})$ is a Dirac delta distribution (δ-distribution). □

Based on Lemma 1, we can adapt the Eq. (12) as:

$$\min_{q(\mathbf{Z}^{1:T} \mid \mathbf{G}^{1:T}), q(\mathbf{Y}^T, \mathbf{Z}^{1:T})} \mathrm{KL}\left[p(\mathbf{Y}^T \mid \mathbf{G}^{1:T}, \mathbf{e}) \parallel q(\mathbf{Y}^T \mid \mathbf{Z}^{1:T})\right] + I(\mathbf{Y}^T; \mathbf{e} \mid \mathbf{Z}^{1:T}). \tag{C.31}$$

Thus, based on Lemma 2, we validate that minimizing Eq. (12) is equivalent to minimizing the upper bound of the OOD generalization error in Eq. (2), *i.e.*,

$$\begin{aligned}
\min_{\boldsymbol{\theta}} \mathcal{L}_{\text{task}} + \alpha \mathcal{L}_{\text{risk}} \Leftrightarrow & \min_{q(\mathbf{Z}^{1:T} \mid \mathbf{G}^{1:T}), q(\mathbf{Y}^T, \mathbf{Z}^{1:T})} \mathrm{KL}\left[p(\mathbf{Y}^T \mid \mathbf{G}^{1:T}, \mathbf{e}) \parallel q(\mathbf{Y}^T \mid \mathbf{Z}^{1:T})\right] \\
& \qquad + I(\mathbf{Y}^T; \mathbf{e} \mid \mathbf{Z}^{1:T}) \\
\geq & \min_{q(\mathbf{Z}^{1:T} \mid \mathbf{G}^{1:T}), q(\mathbf{Y}^T, \mathbf{Z}^{1:T})} \mathrm{KL}\left[p(\mathbf{Y}^T \mid \mathbf{G}^{1:T}, \mathbf{e}) \parallel q(\mathbf{Y}^T \mid \mathbf{Z}^{1:T})\right] \\
\geq & \mathrm{KL}\left[p(\mathbf{Y}^T \mid \mathbf{G}^{1:T}, \mathbf{e}) \parallel q(\mathbf{Y}^T \mid \mathbf{G}^{1:T})\right]. \ (I(\mathbf{Y}^T; \mathbf{e} \mid \mathbf{Z}^{1:T}) \text{ is non-negative})
\end{aligned} \tag{C.32}$$

We conclude the proof for Proposition 4. □

D Experiment Details and Additional Results

D.1 Datasets Details

We use three real-world datasets to evaluate EAGLE on the challenging future link prediction task.

- **COLLAB**[1] [81] is an academic collaboration dataset with papers that were published during 1990-2006 (16 graph snapshots). Nodes and edges represent authors and co-authorship, respectively. Based on the co-authored publication, there are five attributes in edges, including "Data Mining", "Database", "Medical Informatics", "Theory" and "Visualization". We pick "Data Mining" as the shifted attribute. We apply word2vec [59] to extract 32-dimensional node features from paper abstracts. We use 10/1/5 chronological graph snapshots for training, validation, and testing, respectively. The dataset includes 23,035 nodes and 151,790 links in total.
- **Yelp**[2] [75] contains customer reviews on business. Nodes and edges represent customer/business and review behaviors, respectively. Considering categories of business, there are five attributes in edges, including "Pizza", "American (New) Food", "Coffee & Tea", "Sushi Bars" and "Fast Food" from January 2019 to December 2020 (24 graph snapshots). We pick "Pizza" as the shifted attribute. We apply word2vec [59] to extract 32-dimensional node features from reviews. We use 15/1/8 chronological graph snapshots for training, validation, and testing, respectively. The dataset includes 13,095 nodes and 65,375 links in total.

[1] `https://www.aminer.cn/collaboration`

[2] `https://www.yelp.com/dataset`

- **ACT**[3] [45] describes student actions on a MOOC platform within a month (30 graph snapshots). Nodes represent students or targets of actions, edges represent actions. Considering the attributes of different actions, we apply K-Means [29] to cluster the action features into five categories and randomly select a certain category (the 5th cluster) of edges as the shifted attribute. We assign the features of actions to each student or target and expand the original 4-dimensional features to 32 dimensions by a linear function. We use 20/2/8 chronological graph snapshots for training, validation, and testing, respectively. The dataset includes 20,408 nodes and 202,339 links in total.

Statistics of the three datasets are concluded in Table D.1. These three datasets have different time spans and temporal granularity (16 years, 24 months, and 30 days), covering most real-world scenarios. The most challenging dataset for the future link prediction task is the COLLAB. In addition to having the longest time span and the coarsest temporal granularity, it also has the largest difference in the properties of its links.

Table D.1: Statistics of the real-world datasets.

Dataset	# Nodes	# Links	# Graph Snapshots	Temporal Granularity	In-distribution Attributes	Shifted Attribute
COLLAB	23,035	151,790	16	year	Database, Medical Informatics, Theory, Visualization	Data Mining
Yelp	13,095	65,375	24	month	American (New) Food, Fast Food Sushi Bars, Coffee & Tea	Pizza
ACT	20,408	202,339	30	day	Attributes 1-4	Attribute 5

We visualize the distribution shifts in the three real-world dataset with respect to the average neighbor degree (Figure D.1) and the number of interactions (Figure D.2) in training and testing sets. We observe that, there exists a huge difference in terms of the values, trends, *etc.*, between the training set and the testing set, which demonstrates the distribution shifts are heavy. Interestingly, COLLAB has less testing data than its training data, which is common in real-world scenarios, such as not all the co-authorship was established from the beginning. In addition, we notice a drastic drop in Yelp after January 2019 when the COVID-19 outbreak. The sudden change in predictive patterns increases the difficulty of the task. A similar abnormal steep upward trend can also be witnessed in ACT after Day 20, which may be caused by an unknown out-of-distribution event.

(a) COLLAB (b) Yelp (c) ACT

Figure D.1: Visualizations of the average neighbor degree in each graph snapshot.

D.2 Baseline Details

We compare EAGLE with representative GNNs and OOD generalization methods.

- **Static GNNs**: **GAE** [42] is a representative static GNN as the GCN [41] based graph autoencoder; **VGAE** [42] further introduces variational variables into GAE, possessing better generative ability.
- **Dynamic GNNs**: **GCRN** [76] is a representative dynamic GNN following "spatial first, temporal second" convolution mechanism, which firstly adopts GCNs to obtain node embeddings and then a GRU [13] to capture temporal relations; **EvolveGCN** [62] applies an LSTM [31] or GRU

[3] `https://snap.stanford.edu/data/act-mooc.html`

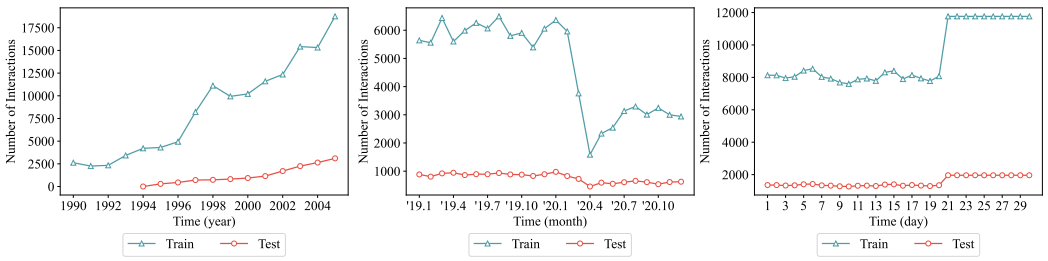

(a) COLLAB (b) Yelp (c) ACT

Figure D.2: Visualizations of the number of interactions in each graph snapshot.

to flexibly evolve the parameters of GCNs instead of modeling the dynamics after deriving node embeddings; **DySAT** [75] models dynamic graph through self-attentions in both structural neighborhoods and temporal dynamics.

- **OOD generalization methods**: **IRM** [3] minimizes the empirical risk to learn an optimal invariant predictor under potential environments; **V-REx** [44] extends the IRM by reweighting the empirical risk to emphasize more on training samples with larger errors; **GroupDRO** [74] reduces the empirical risk gap across training distributions to enhance the robustness when encountering heavy OOD shifts; **DIDA** [94] tackles OOD generalization problem on dynamic graphs for the first time by discovering and utilizing invariant patterns. It is worth noting that, DIDA [94] is the most relative work as our main baseline for comparison.

D.3 Experiment Setting Details

Detailed Settings for Section 4.1.1. Each of the three real-world datasets can be split into several partial dynamic graphs based on their link properties, which demonstrates the multi-attribute relations under the impact of their surrounding environments. We filter out one certain attribute links as the variables under the future shifted environment as the OOD data, and the left links are further divided into training, validation, and testing sets chronologically. The shifted attribute links will only be accessible during the OOD testing stage, which is more practical and challenging in real-world scenarios as the model cannot capture any information about the filtered links during training and validation. Note that, all attribute-related features have been removed after the above operations before feeding to EAGLE. Take the COLLAB dataset for example. There are five attribute links in COLLAB as summarized in Table D.1. We filter out all the links with the attribute "Data Mining", and split the rest of the links into training, validation, and testing sets by positive and negative edge sampling. Then we add the "Data Mining" links into testing sets to make the distribution shifts. Finally, we remove all link attribute information to avoid data leakage.

Detailed Settings for Section 4.1.2. Denote original node features and structures as $\mathbf{X}^t \in \mathbb{R}^{N\times d}$ and $\mathbf{A}^t \in \{0,1\}^{N\times N}$. For each time t, we uniformly sample $p(t)|\mathcal{E}^{t+1}|$ positive links and $(1-p(t))|\mathcal{E}^{t+1}|$ negative links, which are then factorized into shifted features $\mathbf{X}^{t\prime} \in \mathbb{R}^{N\times d}$ while preserving structural property. Original node features and synthesized node features are concatenated as $[\mathbf{X}^t\|\mathbf{X}^{t\prime}]$ as the input. In details, $\mathbf{X}^{t\prime}$ is obtained by training the embeddings with reconstruction loss $\ell(\mathbf{X}^{t\prime}\mathbf{X}^{t\prime\top}, \mathbf{A}^{t+1})$, where $\ell(\cdot)$ refers to the cross-entropy loss function [16]. In this way, we find that the link predictor can achieve satisfying results by using $\mathbf{X}^{t\prime}$ to predict the links in $\mathbf{A}^{t+1}$, which demonstrates that the generated node features have strong correlations with the future underlying environments. The sampling probability $p(t) = \bar{p} + \sigma\cos(t)$, where $\mathbf{X}^{t\prime}$ with higher $p(t)$ will have stronger spurious correlations with future underlying environments. Note that, we apply the $\mathrm{clip}(\cdot)$ function to limit the probability to between 0 and 1. We set $\bar{p}$ to be 0.4, 0.6, and 0.8 for training and 0.1 for testing; set $\sigma = 0.05$ in training and $\sigma = 0$ in testing.

Detailed Settings for Section 4.2. We set the number of nodes $N =$ 2,000 with 10 graph snapshots, where 6/2/2 chronological snapshots are used for training, validation, and testing, respectively. We set $K = 5$ and let $\sigma_{\mathbf{e}}$ represent the proportion of the environments in which the invariant patterns are learned, where higher $\sigma_{\mathbf{e}}$ means more reliable invariant patterns. Node features with respect to different environments are drawn from five multivariate normal distributions $\mathcal{N}(\boldsymbol{\mu}_k; \boldsymbol{\sigma}_k)$. Features

with respect to the invariant patterns will be perturbed slightly, while features with respect to the variant patterns will be perturbed significantly. Here we perturb features by adding Gaussian noise with different degrees. We then construct graph structures based on node feature similarity. Links generated by the node-pair representations under the $\mathbf{e}_5$ are filtered out during the training and validation stages, which is similar to the setting of Section 4.1.1, and they only appear in the testing stage following the proportion constraint $\bar{q}$. Higher $\bar{q}$ means more heavier distribution shifts. $\mathbb{I}_{\text{ACC}}$ denotes the prediction accuracy of the invariant patterns by $\mathbb{I}(\cdot)$. As the environments $\mathbf{e} = \{\mathbf{e}_k\}_{k=1}^{5}$ do not satisfy the permutation invariance property, thus the predicted invariant patterns with respect to $\mathbf{e}$ is hard to evaluate. May wish to set the $\mathbb{I}_{\text{ACC}}$ reports the highest results as we shift the orders of environments in $\mathbf{e}$ to satisfy the predicted invariant patterns better.

D.4 Hyperparameter Sensitivity Analysis

We analyze the sensitivity of the hyperparameters α and β, which act as the trade-off for loss in Eq. (16). The hyperparameter α is chosen from $\{10^{-3}, 10^{-2}, 10^{-1}, 10^{0}, 10^{1}\}$, and β is chosen from $\{10^{-6}, 10^{-5}, 10^{-4}, 10^{-3}, 10^{-2}\}$. We conduct analysis on three real-world datasets and report results in Figure D.3 and Figure D.4. Results demonstrate that the task performance experiences a significant decline in most datasets when the values of α and β are too large or too small. We can draw a conclusion that α acts as a balance factor between exploiting the spatio-temporal invariant patterns for out-of-distribution prediction and generalizing to diverse latent environments with respect to variant patterns. β plays a role in balancing the trade-off between modeling the environment and inferring the environment distribution as a bi-level optimization. In conclusion, different combinations of hyperparameters lead to varying task performance, and we follow the tradition of reporting the best task performance with standard deviations.

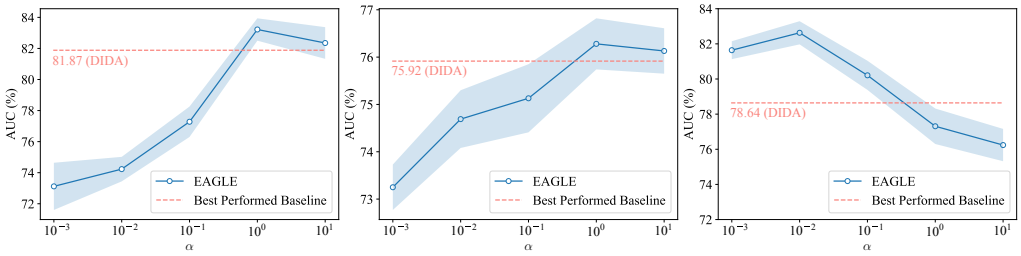

(a) COLLAB (b) Yelp (c) ACT

Figure D.3: Sensitivity analysis of the hyperparameter α on three real-world datasets. The solid line shows the average AUC (%) in the testing stage and the light blue area represents standard deviations. The dashed line represents the average AUC (%) of the best-performed baseline.

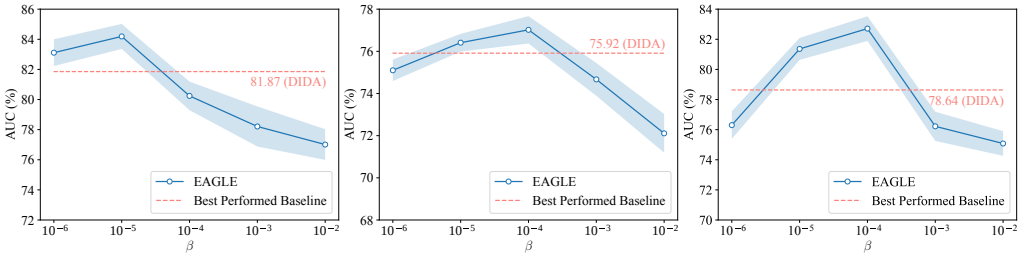

(a) COLLAB (b) Yelp (c) ACT

Figure D.4: Sensitivity analysis of the hyperparameter β on three real-world datasets. The solid line shows the average AUC (%) in the testing stage and the light blue area represents standard deviations. The dashed line represents the average AUC (%) of the best-performed baseline.

D.5 Intervention Efficiency Analysis

From the results of complexity analysis in Appendix B, we believe the computational complexity bottleneck of EAGLE lies in the spatio-temporal causal intervention mechanism. In this case, we analyze the intervention efficiency in the following two aspects.

Intervention Ratio. We perform node-wisely causal interventions as in Eq. (15). However, executing interventions for all nodes in each epoch is time-consuming. Thus, we propose randomly selecting nodes and performing interventions according to a certain ratio. Let the intervention ratio represent the ratio of the number of intervened nodes to the total number of nodes $|\mathcal{V}|$. Figure D.5 shows the changes in task performance (AUC %) and the training time as the intervention ratio increases. We observe the AUC increases, proving that the spatio-temporal causal intervention mechanism is more effective in solving the OOD generalization problem with more intervened nodes. In addition, we notice a jump in the growth rate of AUC on three datasets at the ratio of 0.6, which indicates the most suitable intervention ratio while maintaining an acceptable training time cost.

Mixing Ratio. The intervention set $\mathbf{s}_v$ is sampled from $\mathcal{S}_{\text{ob}} \cup \mathcal{S}_{\text{ge}}$. While $\mathcal{S}_{\text{ob}}$ has been already prepared after we model the environments in Section 3.1, the $\mathcal{S}_{\text{ge}}$ requires instantly generating, which may be a burden on the intervention efficiency. Let the maxing ratio represent the ratio of the number of observed environment samples to the number of generated environment samples. Figure D.6 shows the changes in task performance (AUC %) and the training time as the mixing ratio increases. Different from the trend in Figure D.5, AUC reached the maximum value at different ratios on the three datasets, and when the ratio is too large or small, the model performs poorly, indicating that different datasets have varying preferences for mixing ratio settings. In addition, we observe the variation in training time is not significant, verifying that although $\mathcal{S}_{\text{ob}}$ needs to be generated instantly, its time cost is acceptable still, and we should pay more attention on the optimal mixing ratio.

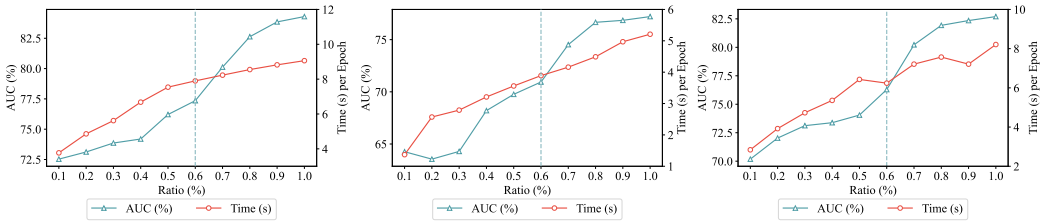

(a) COLLAB (b) Yelp (c) ACT

Figure D.5: Intervention efficiency analysis on the intervention ratio. The vertical dashed line indicates the most suitable intervention ratio while maintaining an acceptable training time cost.

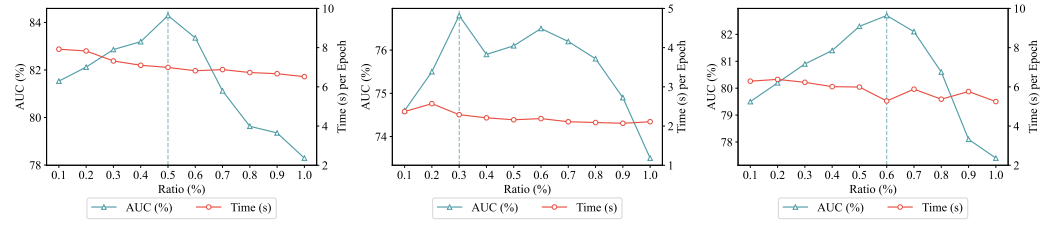

(a) COLLAB (b) Yelp (c) ACT

Figure D.6: Intervention efficiency analysis on the mixing ratio. The vertical dashed line indicates the ratio when AUC reaches the maximum value.

D.6 Additional Analysis of Section 4.1

We visualize Table 1 and Table 2 in Section 4.1 to provide additional analysis. We have concluded in Section 4.1 that the baselines own a strong fitting ability but weak generalization ability between the distribution shifts settings. In addition to visualizing the task performance (AUC %), Figure D.7

annotates the decrease of AUC under each baseline method, where the horizontal dashed line represents the AUC decrease of our EAGLE. The smaller the decrease, the stronger the control ability under the impact of out-of-distribution shifts. We can observe that on the vast majority of datasets, our method can improve task performance in both *w/o OOD* and *w/ OOD* scenarios while minimizing AUC decrease. Our control over AUC decrease exceeds the baseline except for GAE and GCRN in the vast majority of cases. For the above two baseline methods, although they have better control ability over AUC decrease than our method, the premise is that their task performance is inherently poor. In addition, our method achieves the most excellent task performance on the ACT dataset, which can explain the unsatisfying but acceptable AUC decrease control. In summary, in addition to evaluating the advantages of our EAGLE in terms of task performance and generalization ability, which is the most topic-relative and common, our EAGLE also maintains the ability to reduce the impact of OOD on task performance.

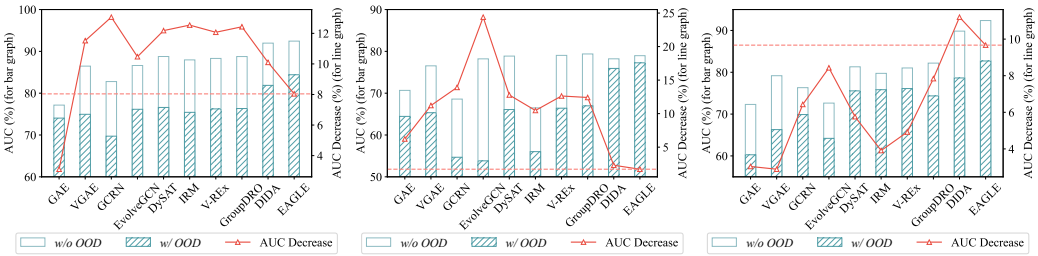

(a) COLLAB (b) Yelp (c) ACT

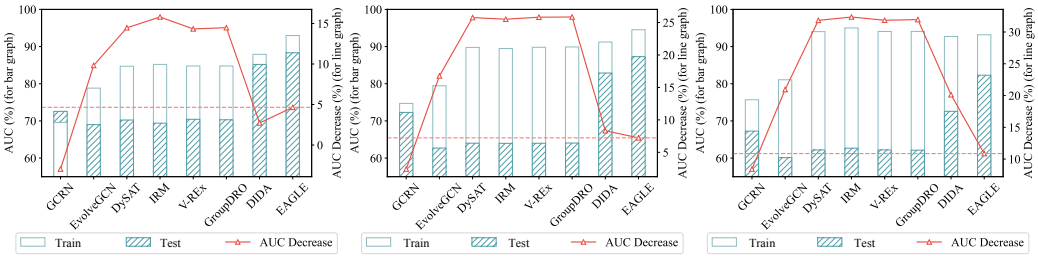

(d) COLLAB ($\bar{p} = 0.4$) (e) COLLAB ($\bar{p} = 0.6$) (f) COLLAB ($\bar{p} = 0.8$)

Figure D.7: Additional analysis of the performance on future link prediction.

D.7 Additional Results of Section 4.2

Section 4.2 reports the results when $\bar{q} = 0.8$. Here we report the additional results when $\bar{q} = 0.4$ and 0.6 in Figure D.8. All detailed results are summarized in Table D.2. A similar trend can be observed as we report in Section 4.2 that as $\sigma_{\mathbf{e}}$ increases, the performance of EAGLE shows a significant increase while narrowing the gap between *w/o OOD* and *w/ OOD* scenarios. Although DIDA [94] also shows an upward trend, its growth rate is much more gradual, which indicates that DIDA [94] is difficult to perceive changes in the underlying environments caused by different $\sigma_{\mathbf{e}}$ as it is incapable of modeling the environments, thus cannot achieve satisfying generalization performance. In addition, we also notice a positive correlation between $\mathbb{I}_{\text{ACC}}$ and the AUC, which verifies the improvements are attributed to the proper recognition of the invariant patterns by $\mathbb{I}(\cdot)$. In conclusion, our EAGLE can exploit more reliable invariant patterns, thus performing high-quality invariant learning and efficient causal interventions, and achieving better generalization ability.

E Implementation Details

E.1 Training and Evaluation

Training Settings. The number of training epochs for optimizing our proposed method and all baselines is set to 1000. We adopt the early stopping strategy, *i.e.*, stop training if the performance

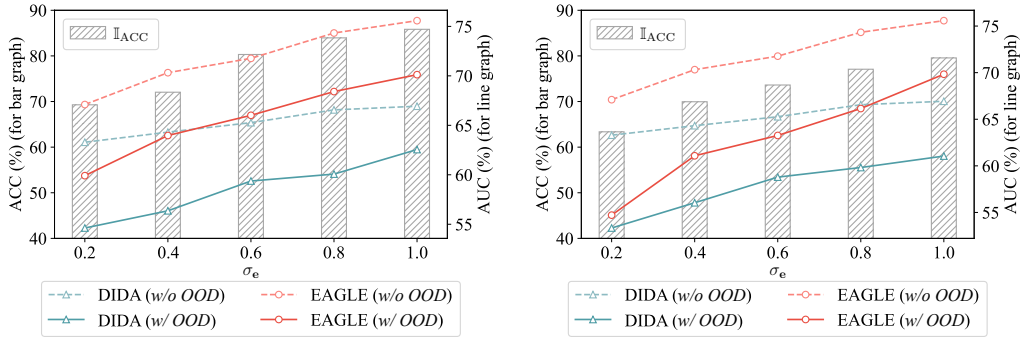

(a) $\bar{q} = 0.4$ (b) $\bar{q} = 0.6$

Figure D.8: Additional results on the effects of invariant pattern recognition.

Table D.2: AUC score (% ± standard deviation) of future link prediction task on synthetic datasets. *w/o OOD* and *w/ OOD* denote testing without and with distribution shifts. $\mathbb{I}_{\text{ACC}}$ is reported in the accuracy score). The best results are shown in **bold** and the runner-ups are underlined.

Shift Degree		—	$\bar{q} = 0.4$		$\bar{q} = 0.6$		$\bar{q} = 0.8$	
σ_e	**Model**	*w/o OOD*	*w/ OOD*	$\mathbb{I}_{\text{ACC}}$	*w/ OOD*	$\mathbb{I}_{\text{ACC}}$	*w/ OOD*	$\mathbb{I}_{\text{ACC}}$
0.2	DIDA [94]	63.29±0.35	54.62±0.92	—	53.33±1.01	—	52.87±1.28	—
	EAGLE	67.10±0.23	59.91±1.18	69.28±1.59	54.71±1.29	63.36±1.74	54.26±1.31	59.79±1.37
0.4	DIDA [94]	64.31±0.34	56.36±0.98	—	56.04±1.13	—	55.89±1.24	—
	EAGLE	70.32±0.27	63.97±0.82	72.04±1.34	61.08±1.02	69.95±1.30	58.40±1.12	63.88±1.36
0.6	DIDA [94]	65.27±0.41	59.37±0.87	—	58.79±0.97	—	57.35±1.19	—
	EAGLE	71.77±0.38	66.01±0.74	80.31±1.52	63.26±0.64	73.62±1.41	63.11±0.78	69.30±1.50
0.8	DIDA [94]	66.56±0.39	60.07±0.89	—	59.82±1.05	—	59.20±1.03	—
	EAGLE	74.33±0.29	68.41±0.72	83.95±1.66	66.15±0.69	77.08±1.73	65.82±0.81	72.59±1.46
1.0	DIDA [94]	66.93±0.18	62.55±0.85	—	61.05±0.93	—	60.33±1.17	—
	EAGLE	**75.58±0.40**	**70.12±0.91**	**85.83±1.54**	**69.83±0.93**	**79.56±1.65**	**68.09±0.97**	**74.16±1.21**

on the validation set does not improve for 50 epochs. For our EAGLE, the hyperparameter α is chosen from $\{10^{-3}, 10^{-2}, 10^{-1}, 10^{0}, 10^{1}\}$, and β is chosen from $\{10^{-6}, 10^{-5}, 10^{-4}, 10^{-3}, 10^{-2}\}$. The intervention ratio and the mixing ratio are carefully tuned for each dataset. For other parameters, we adopt the Adam optimizer [40] with an appropriate learning rate and weight decay for each dataset and adopt the grid search for the best performance using the validation split. All parameters are randomly initiated, which is especially important for $\mathbf{W}_k$ in Eq. (3) that ensures the difference in each environment embedding space. The K channels will still remain orthogonal during training as we conduct discrete environment disentangling iteratively. This helps the recognition of invariant/variant patterns mainly because we guarantee there is no overlap between environments.

Evaluation. According to respective experiment settings, we randomly split the dynamic datasets into training, validation, and testing chronological sets. We sample negative links from nodes that do not have links, and the negative links for validation and testing sets are kept the same for all baseline methods and ours. We set the number of positive links to the same as the negative links. We use the Area under the ROC Curve (AUC) [7] as the evaluation metric. As we focus on the future link prediction task, we use the inner product of a pair of learned node representations to predict the occurrence of links, *i.e.*, we implement the link predictor $g(\cdot)$ as the inner product of hidden embeddings, which is commonly applied in classic future link prediction tasks. The biased training technique is adopted following [9]. We use the cross-entropy loss as the loss function $\ell(\cdot)$. The activation function is LeakyReLU [1]. We randomly run all the experiments five times, and report the average results with standard deviations.

E.2 Baseline Implementation Details

We provide the baseline methods implementations with respective licenses as follows.

- GAE [42]: `https://github.com/DaehanKim/vgae_pytorch` with MIT License.
- VGAE [42]: `https://github.com/DaehanKim/vgae_pytorch` with MIT License.
- GCRN [76]: `https://github.com/youngjoo-epfl/gconvRNN` with MIT License.
- EvolveGCN [62]: `https://github.com/IBM/EvolveGCN` with Apache-2.0 License.
- DySAT [75]: `https://github.com/FeiGSSS/DySAT_pytorch` with license unspecified.
- IRM [3]: `https://github.com/facebookresearch/InvariantRiskMinimization` with CC BY-NC 4.0 License.
- V-REx [44]: `https://github.com/capybaralet/REx_code_release` with license unspecified.
- GroupDRO [74]: `https://github.com/kohpangwei/group_DRO` with MIT License.
- DIDA [94]: `https://github.com/wondergo2017/DIDA` with license unspecified.

The parameters of baseline methods are set as the suggested value in their papers or carefully tuned for fairness.

E.3 Configurations

We conduct the experiments with:

- Operating System: Ubuntu 20.04 LTS.
- CPU: Intel(R) Xeon(R) Platinum 8358 CPU@2.60GHz with 1TB DDR4 of Memory.
- GPU: NVIDIA Tesla A100 SMX4 with 40GB of Memory.
- Software: CUDA 10.1, Python 3.8.12, PyTorch [63] 1.9.1, PyTorch Geometric [20] 2.0.1.

F Further Discussions

F.1 Further Analysis on SCM Model

We provide further analysis of the intrinsic cause of the out-of-distribution shifts. From the causal-based theories [64, 65, 66], we formulate the generation process of static graphs and dynamic graphs with the Structural Causal Model (SCM) [64] in Figure F.1, where the arrow between variables denotes causal dependencies. It is widely accepted in the OOD generalization works [22, 3, 72, 87, 11, 2, 60] that the correlations between labels and certain parts of the latent features are invariant across data distributions in training and testing, while the other parts of the features are variant. The invariant part is also called the causal part (C) and the variant part is also called the spurious part (S).

Qualitative Analysis. In the SCM model on static graphs, $C \rightarrow \mathbf{G} \leftarrow S$ demonstrates that the invariant part and variant part jointly decide the generation of the graphs, while $C \rightarrow \mathbf{Y}$ denotes the label is solely determined by the causal part. However, there exists the spurious correlation $C \dashleftarrow\dashrightarrow S$ in certain distributions that would lead to a backdoor causal path $S \dashrightarrow C \rightarrow \mathbf{Y}$ so that the variant part and the label are correlated statistically. As the variant part changes in the testing distributions caused by different environments $\mathbf{e}$, the predictive patterns built on the spurious correlations expired. For the same reason, similar spurious correlation $C^t \dashleftarrow\dashrightarrow S^t$ exists on dynamic graphs within a single graph snapshot, which opens the backdoor causal path $S^t \dashrightarrow C^t \rightarrow \mathbf{Y}^t$. Especially, as we have captured the temporal dynamics between each graph snapshot, the variant part in the previous time slice may also establish spurious correlations with the invariant part at present time, *i.e.*, $C^{t-1} \dashleftarrow\dashrightarrow S^t$, leading to $S^{t-1} \dashrightarrow C^t \rightarrow \mathbf{Y}^t$, which is a unique phenomenon in the dynamic scenarios. Hence, we propose to get rid of the spurious correlations within and between graph snapshots by investigating the latent environment variable $\mathbf{e}$, encouraging the model to rely on the spatio-temporal invariant patterns to make predictions, and thus handle the distribution shifts.

Further Analysis of Assumption 1. The causal inference theories [64, 65, 66] propose to get rid of the spurious correlations by blocking the backdoor path with do-calculus, which would remove all causal dependencies on the intervened variables. Particularly, we intervene in the variant parts on all graph snapshots, *i.e.*, $\mathrm{do}(S^t)$, and thus the spurious correlations within and between graph snapshots can be filtered out. This encourages the two conditions in Assumption 1 to be satisfied: the Invariance

Property will be satisfied if the spurious correlations $S^{t-1} \not\leftarrow \not\rightarrow C^t \not\leftarrow \not\rightarrow S^t$ are removed and the label will be solely decided by the invariant part $C^t \rightarrow \mathbf{Y}^t$, which also satisfies the Sufficient Condition. In this case, we can minimize the variance of the empirical risks under diverse potential environments, while encouraging the model to make predictions of the spatio-temporal invariant patterns.

Further Explanations of the Toy Example. From the above analysis, we can further explain the toy example in Figure 1(a). The prediction model has captured the spurious correlations between "coffee" and the "cold drink", which caused the false prediction of buying an Iced Americano in the winter. By applying our environment-ware EAGLE, the prediction model can perceive the environments of seasons through the neighbors around the central node, *i.e.*, perceiving the winter season by learning the observed interactions between the user and the thick clothing. Thus encouraging the model to rely on the exploited spatio-temporal invariant patterns, *i.e.*, "the user buys coffee", to make the correct prediction on the Hot Latte by considering underlying environments.

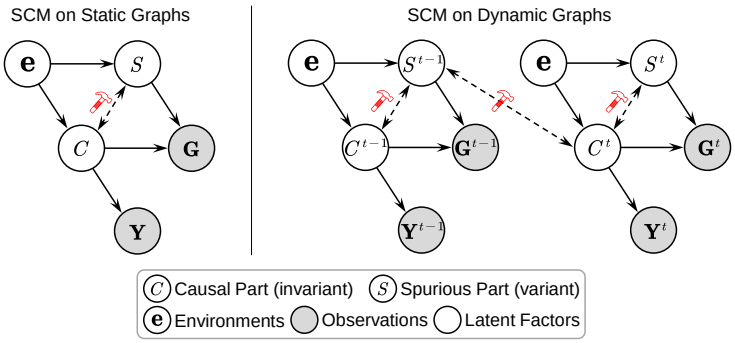

Figure F.1: The SCM model on static graphs and dynamic graphs.

F.2 Further Understanding of Environments

Environments on dynamic graphs are latent factors, where there are no accessible ground-truth environment labels in the real world, leading to the lack of explainability. In order to improve the explainability of the environment, and patterns the EA-DGNN learns, we have provided some real-world examples to make explanations (Section 3.1). The key insight lies that, the formation of real-world dynamic graphs typically follows a complex process under the impact of latent environments, causing the relationships to be multi-attribute. To model diverse spatio-temporal environments, the ego-graphs of each node need to be disentangled and processed in different embedding spaces.

An Easy-to-Understand Example: the Social Networks. The relationships between the central node and its neighbor nodes, which may be classmates, colleagues, *etc.*, are formed under the influence of different surrounding environments. For example, the relationship between classmates is formed in the "school" environment, which is a compound of "classmates", "teachers", "staff", *etc.*, and the relationship between colleagues is formed in the "working" environment, *etc.* Multiple relationships are compounded into a single edge and change over time. In order to model such multiple environments, we propose multi-channel environments disentangling to represent different semantic relationships in K embedding spaces. For example, the 1-st embedding represents the "classmate" relationship, and the 2-nd embedding space represents the "colleague" relationship, *etc.* Thus, EA-DGNN realizes the perception of multiple surrounding environments and encodes spatio-temporal environment information into node representations.

F.3 Further Understanding of the Multi-Label

Understanding. We do not require ground-truth environment labels in our EAGLE. The environments on dynamic graphs are latent factors, where there are no accessible ground-truth environment labels that have practical meanings in the real world. This is also why conventional OOD generalization baselines on images, text, *etc.* have poor performance (Section 4.1) in graphs as they must rely on the ground-truth environment labels to generalize. In our work, the multi-label $\mathbf{y}$ in Section 3.2 is mixed up with time index t and environment index k, indicating which environment index under which time index $\mathbf{z}$ belongs. It can be seen as our inferred label of environments.

Example. If there exist K environments and T graph snapshots, we first initialize a zero matrix of the shape $K \times T$. Then we mark the value in position (k, t) to be 1 and reshape the matrix into the 1-dimension vector $\mathbf{y}$, indicating the multi-label of $\mathbf{z}$ for the k-th environment at time t.

Role. The multi-labels are used with $\mathbf{z}$ to infer environments by ECVAE, where the multi-label is concatenated with its corresponding $\mathbf{z}$ to realize conditional variational inference. We can then instantiate environments by generating samples from the inferred distribution with a given one-hot multi-label. This can be regarded as the data augmentation of the environment samples under the guidance of the inferred prior distribution $q_\phi(\mathbf{e} \mid \mathbf{z}, \mathbf{y})$, which helps improve the generalization ability.

F.4 Further Understanding of Proposition 2

Targets and Principles. Proposition 2 provides a solution to obtain the optimal $\mathbb{I}^\star(\cdot)$ in Assumption 1 with theoretical proof in Appendix C.2. In fact, Proposition 2 solves a dynamic programming problem by optimizing the state transition equation $\mathbb{I}(i, j)$. Given $\mathrm{Var}(\mathbf{z}_v^{\mathbf{e}\prime}) \in \mathbb{R}^K$ as the representation variance of node v in each environment across times, the target is to find a partition dividing all environment patterns into invariant and variant types, so as to maximize the difference between the variance means.

A Conceptual Example. If $\mathrm{Var}(\mathbf{z}_v^{\mathbf{e}\prime})$ of node v is [0.1, 0.2, 0.3, 0.4, 0.9], then the optimal partition is [0.1, 0.2, 0.3, 0,4] and [0.9] (with a larger mean difference) rather than [0.1, 0.2, 0.3] and [0.4, 0.9]. An optimal partition can always be found for each node, which greatly helps the patterns discrimination and fine-grained causal interventions, improving the generalization ability, and is one of our main advantages compared with DIDA [94].

Proposition 2 intuitively illustrates a feasible implementation for the optimal $\mathbb{I}^\star(\cdot)$, providing an ideal optimizing start point. Note that, Proposition 2 itself cannot fully guarantee the global accuracy of identifying the $\mathbb{I}^\star(\cdot)$, but should optimize along with the $\mathcal{L}_{\mathrm{risk}}$ loss (Eq.(14)), which provides theoretical ensure.

F.5 Further Discussions Compared with DIDA

The difference between our EAGLEand DIDA [94], and EAGLE's main advantages are:

- **Modeling Environments.** EAGLE is the first to explicitly model latent environments on dynamic graphs by variational inference. DIDA [94] neglects to model complex environments, which weakens its ability to identify invariant patterns.
- **Representation Learning.** EAGLE learns node embeddings by K-channel environments disentangling and spatio-temporal convolutions, which helps better understand multi-attribute relations. DIDA [94] learns with single channel convolutions with an attention mechanism.
- **Invariant Learning.** EAGLE discriminates spatio-temporal invariant patterns by the theoretically supported $\mathbb{I}^\star(\cdot)$ for each node individually, leading to better removal of spurious correlations. DIDA [94] divides invariant/variant parts heuristicly with a minus operation for all nodes.
- **Causal Intervention.** EAGLE performs fine-grained causal interventions with both observed and generated environment samples, better minimizing the variance of extrapolation risks, and generalizing to unseen distributions better. DIDA [94] intervenes coarse-grainedly with only observed samples.

F.6 Further Related Work

Dynamic Graph Learning. Extensive research [70, 4] address the challenges of learning on dynamic graphs, which consist of multiple graph snapshots at different times. Dynamic graph neural networks (DGNNs) are widely adopted to learn dynamic graphs by intrinsically modeling both spatial and temporal patterns, which can be divided into two main categories: spatial-first methods and temporal-first methods. The spatial-first methods [88, 28, 76] first adopt vanilla GNNs to model spatial patterns for each graph snapshot, followed by sequential-based models like RNNs [58] or LSTMs [31], to capture temporal relations. In comparison, temporal-first DGNNs [84, 73] model dynamics in advance with temporal encoding mechanisms [32], and then conduct convolutions of message-passing and aggregating on each single graph with GNNs. Dynamic graph learning has been widely utilized for prediction tasks like disease transmission prediction [38], dynamic recommender system [90],

social relation prediction [85], *etc.* However, most existing works fail to generalize under distribution shifts. DIDA [94] is the sole prior work that addresses distribution shifts on dynamic graphs with an intervention mechanism. But DIDA [94] neglects to model the complex environments on dynamic graphs, which is crucial in tackling distribution shifts. We also experimentally validate the advantage of our method compared with DIDA [94].

Out-of-Distribution Generalization. Most machine learning methods are built on the I.I.D. hypothesis, *i.e.*, training and testing data follow the independent and identical distribution, which can hardly be satisfied in real-world scenarios [77], as the generation and collection process of data are affected by many latent factors [71, 3]. The non-I.I.D. distribution results in a significant decline of model performance, highlighting the urgency to investigate generalized learning methods for out-of-distribution (OOD) shifts, especially for high-stake downstream applications, like autonomous driving [15], financial system [62], *etc.* OOD generalization has been extensively studied in both academia and industry covering various areas [77, 92, 30] and we mainly focus on OOD generalization on graphs [50]. Most graph-targeted works concentrate on node-level or graph-level tasks on static graphs [98, 18, 49, 86, 52, 12, 87], targeting at solving the problems of graph OOD generalization for drugs, molecules, *etc.*, which is identified as one key challenge in AI for science (AI4Science). Another main category of works elaborates systematic benchmarks for graph OOD generalization evaluation [26, 17, 36]. However, there lack of further research on dynamic graphs with more complicated shift patterns caused by spatio-temporal varying latent environments, which is our main concern.

Invariant Learning. Deep learning models tend to capture predictive correlations behind observed samples, while the learned patterns are not always consistent with in-the-wild extrapolation. Invariant learning aims to exploit the less variant patterns that lead to informative and discriminative representations for stable prediction [14, 46, 95]. Supporting by disentangled learning theories and causal learning theories, invariant learning tackles the OOD generalization problem from a more theoretical perspective, revealing a promising power. Disentangle-based methods [5, 55] learn representations by separating semantic factors of variations in data, making it easier to distinguish invariant factors and establish reliable correlations. Causal-based methods [22, 3, 72, 87, 11, 2, 60] utilize Structural Causal Model (SCM) [64] to filter out spurious correlations by intervention or counterfactual with do-calculus [65, 66] and strengthen the invariant causal patterns. However, the invariant learning method of node-level tasks on dynamic graphs is underexplored, mainly due to its complexity in analyzing both spatial and temporal invariant patterns.

Disentangled Representation Learning. Disentangled Representation Learning (DRL) is a paradigm that inspires a model with the capability to discriminate and disentangle latent factors intrinsic to the observable data. The fundamental objective of DRL is to separate latent factors of variation into distinct variables endowed with semantic significance. This helps to improve the generalization capacity, explainability, and robustness, *etc.* in a wide range of scenarios. Following [83], we categorize existing DRL works into traditional statistical approaches, VAE-based approaches, GAN-based approaches, hierarchical approaches, and other methods. Specifically, applying DRL to graphs results in benefits and advantages in graph tasks. DisenGCN [56], FactorGCN [89], DGCL [48], *etc.* decompose the input graph into segments for disentangled representations, which inspire our work on environment disentangling.